J. Phys. B: At. Mol. Opt. Phys. 26 (1993) 2555–2573. Printed in the UK

A hyperspherical close-coupling calculation of photoionization from the He atom, Li^+ and C^{4+} ions: I. Below the $N = 2$ threshold

Bin Zhou†, C D Lin†, Jian-Zhi Tang‡§, Shinichi Watanabe‡ and Michio Matsuzawa‡

† Department of Physics, Kansas State University, Manhattan, Kansas 66506, USA
‡ Department of Applied Physics and Chemistry, The University of Electro-Communications, Chofu-shi, Tokyo 182, Japan

Received 11 February 1993

Abstract. We give a detailed account of the formulation of the recently developed hyperspherical close-coupling (HSCC) method. Using this method, we have made calculations of photoionization cross sections for the He atom and He-like ions, Li^+ and C^{4+} below the $N = 2$ (the inner electron's principal quantum number) threshold. From analysing the photoionization cross section spectra and resonance structures of the two-electron systems with different nuclear charge, the effect of the interplay between the electron–nucleus and electron–electron interactions on doubly excited states is studied.

1. Introductions

Since the first observation of doubly excited states in helium in the early 1960s (Madden and Codling 1963), great progress has been made in understanding the nature of electron–electron correlation in doubly excited states. As the simplest many-electron system, helium has received most attention both experimentally and theoretically in the study of doubly excited states. With the improving performance of synchrotron radiation sources, a great deal of experimental efforts have been devoted to precision measurements of photoionization cross sections in the vicinity of autoionizing doubly excited states. In particular, the photon energy range of 59–73 eV, which covers the doubly excited states associated with $N = 2$ and three manifolds of He, have been most extensively studied (e.g. Woodruff and Samson 1982, Morgan and Ederer 1984, Lindle *et al* 1985, 1987, Zubek *et al* 1989, Domke *et al* 1991, 1992). The resolution of experimental measurement has reached to as high as 4 meV, giving details of resonance profiles of high lying doubly excited states and uncovering weak resonances which had not been observed before (Domke *et al* 1991, 1992). Along with the rapid advance in the experimental study, theoretical understandings of doubly excited states have reached a new level, since the early work of Cooper *et al* (1963). A new set of approximate quantum numbers K, T, A, characterizing radial and angular correlations of the electron–electron interaction, have been introduced and successfully employed in the classification of doubly excited states (Herrick 1983, Lin 1986 and references therein). Energy positions and autoionization widths have been calculated

§ Present address: Atomic Physics Laboratory, The Institute of Physical and Chemical Research (RIKEN), Hirosawa 2-1, Wako-shi, Saitama 351-01, Japan.

0953-4075/93/162555+19$07.50 © 1993 IOP Publishing Ltd

and compared with experimental results where available (Lipsky *et al* 1977, Bachau *et al* 1991, Chung 1972, Chung and Davis 1980, Ho 1981, 1979, Ho and Callaway 1985). Calculations of photoionization cross sections, the asymmetry parameter of the photoelectron angular distribution, for photon energies below the $N = 2$ threshold, as well as between the $N = 2$ and $N = 3$ thresholds, have been performed, utilizing various approaches, such as the R-matrix method (e.g. Scott and Burke 1984), the many-body perturbation theory (e.g. Salomonson *et al* 1989) and the variational method using the L^2 basis set (Sánchez and Martín 1990, Moccia and Spizzo 1987, 1991). Recently, Tang *et al* (1992a, b, c) have demonstrated the use of the close-coupling method in the hyperspherical coordinates (HSCC) in producing highly accurate results of both the doubly excited state energy positions and photoionization cross sections of He.

A well known fact about doubly excited states in He is that the strong electron–electron interaction is responsible for the failure of the independent electron model and accounts for all new features seen in doubly excited states. If nuclear charge increases, the relative importance of the electron–electron interaction is lessened in the face of overwhelming electron–nucleus Coulomb interaction, but the independent electron model is still inadequate because the first order solutions are degenerate due to the $O(4)$ symmetry of the Coulomb interaction. It is desirable to make a systematic comparative study of the He-like ion series to see how the interplay between the two interactions affects the spectra of doubly excited states as the nuclear charge Z varies. To this end, in this paper we report an extensive calculation of photoionization cross sections of helium, the lithium 1+ ion, and the carbon 4+ ion, with Z varying from 2, to 3 and 6, in the energy ranges below the $N = 2$ threshold $\mathrm{I\!P}_2$ (we shall adopt the notation $\mathrm{I\!P}_N$ for the ionization potential limit which equals to the total energy of the system required to ionize one electron while leaving another in the state of principal quantum number N) in the framework of the HSCC method. The results for energies between the $N = 2$ threshold $\mathrm{I\!P}_2$ and the $N = 3$ threshold $\mathrm{I\!P}_3$ are reported in the following paper (Zhou and Lin 1993). From studying the photoionization cross sections of the He-like series, we uncover some interesting trends in physical quantities such as the Fano shape parameter q and widths of doubly excited states, as a function of Z.

Compared with the neutral atomic helium and the hydrogen negative ion, both experimental and theoretical studies of photoionization of the He-like positive ions are far from complete. Theoretically, numerous studies on energy positions, and autoionization widths to some extent, of doubly excited states in the He-like series have been carried out (Lipsky *et al* 1977, Bachau *et al* 1991, Chung 1972, Chung and Davis 1980, Ho 1979, 1981) using variational type calculations. Besides the result of the Fano parameter q for the three lowest $^1P^o$ autoionization states of the $N = 2$ manifold for Li^+ by Bhatia and Temkin (1983), Sánchez and Martín (1990) made a more systematic study of Li^+ and other He-like systems below the $N = 2$ threshold. On the experimental side, doubly excited states of He-like positive ions are mainly studied in atomic collision experiments, where energy positions and widths of doubly excited states can be determined. Experiments on the photoionization of the He-like positive ions are scarce: the lonely example was the measurement of the photoabsorption spectrum below the $N = 2$ threshold for Li^+ in a laser-produced plasma by Carroll and Kennedy (1977). However, with the advance in ion sources and new storage rings for heavy ions, direct measurements of photoionization cross sections for singly or multiply charged ions are being planned. Thus, the photoionization cross sections presented in this and the subsequent paper may also serve as a timely stimulation for future experiments.

The hyperspherical coordinates have been successfully utilized in describing the properties of doubly excited states of two electron systems since their introduction to atomic

physics in the late 1960s (Macek 1968). In the most widely used adiabatic approximation, the hyperradius R is treated as an adiabatic parameter, analogous to the internuclear distance in the Born–Oppenheimer approximation for diatomic molecules, and the two-electron Schrödinger equation is solved at different values of hyperradius. This approach, which gives the adiabatic potentials and two-electron wavefunctions, has played a prominent role in the classification of doubly excited states as well as the visualization of electron–electron correlations in these states (Lin 1986). However, compared with other methods the adiabatic approach has failed to provide more precise energy positions and widths of doubly excited states. The lack of accuracy of the adiabatic approach stems from two main reasons: (i) the couplings among different adiabatic channels, significant in the avoided crossing region, are difficult to handle numerically; (ii) in the asymptotical region, i.e. when the two electrons are well separated in space, the adiabatic channels in the hyperspherical coordinates have spurious couplings proportional to R^{-1} (Macek 1985), since they are not suitable for describing dissociative channels. Despite these difficulties, there have been some efforts to directly solve coupled adiabatic hyperradial equations (Sadeghpour 1992).

In the present HSCC method, the above mentioned difficulties of the adiabatic approximation are overcome respectively by employing the diabatic-by-sector technique (DBS) and the two dimensional frame transformation. The DBS technique, which has already been extensively used in treating reactive scatterings by quantum chemists (e.g. Lepetit *et al* 1986), is a simple but rather general technique in solving coupled differential equations. By the frame transformation, the wavefunctions calculated in hyperspherical coordinates in the inner region are matched to the asymptotic physical solutions in the independent electron coordinates (Christensen-Dalsgaard 1984).

In this work we neglect the spin–orbit interaction, therefore the atomic states are designated by $^{2S+1}L^{\pi}$, with the total angular momentum L, total spin S and parity π. Only final $^1P^o$ states are reached from the ground state $^1S^e$ by photoabsorption within the dipole approximation. Besides the global symmetry represented by L, S and π, it has been shown that doubly excited states are properly classified by a set of approximate quantum numbers K, T and A which describe the properties of the electron–electron correlation (Herrick 1983, Lin 1986). These quantum numbers are complemented by two other approximate quantum numbers N and n, which are the principal quantum numbers of the inner and outer electrons in the independent electron picture. These quantum numbers will be used here to designate doubly excited states calculated. The value of T, the projection of the total angular momentum L onto the interelectronic axis, can take $[0, 1, \ldots, \min(L, N-1)]$. The value of K, which is related to the angle between the Runge–Lenz vectors of the two electron orbitals, is assigned by $[(N-T-1), (N-T-3), \ldots, -(N-T-1)]$. The quantum number A is used to characterize the radial correlation between the two electrons: when the two-electron wavefunction is concentrated mainly near the potential ridge ($r_1 \approx r_2$) A can take either $+1$ or -1 depending on whether the wavefunction has an antinode or a node right on the potential ridge; when the two-electron wavefunction is located mostly in the potential valleys ($r_1 \ll r_2$ or $r_1 \gg r_2$) A is assigned to be zero. Doubly excited states having the same correlation quantum numbers K, T, A have similar internal electronic structures and physical properties, with little dependence on other quantum numbers. A more detailed discussion of these quantum numbers can be found in Lin (1986).

The rest of the paper is organized as follows: in the next section, we will give a detailed description of the HSCC method, with emphasis on the channel basis calculation, the DBS technique and the frame transformation. The technical details of the present calculation and the analysis of the calculated spectra will be explained in sections 3 and 4 respectively while results and discussions of photoionization cross sections for energies below the $N = 2$

threshold will be given in section 5. A brief conclusion is given in the last section 6. As the second part of the series, results and discussions of photoionization cross section in the energy range between the $N = 2$ and $N = 3$ thresholds are presented in the following paper. Atomic units are used throughout unless stated otherwise.

2. Theory: the HSCC method

Assume the nucleus to be infinitely massive, the Schrödinger equation for a two electron atomic system with nuclear charge Z and total energy E in the independent electron coordinates is

$$\left[-\frac{\nabla_1^2}{2} - \frac{\nabla_2^2}{2} - \frac{Z}{r_1} - \frac{Z}{r_2} + \frac{1}{r_{12}}\right]\psi(\boldsymbol{r}_1, \boldsymbol{r}_2) = E\psi(\boldsymbol{r}_1, \boldsymbol{r}_2). \tag{1}$$

In the hyperspherical coordinates, the electron coordinates r_i are replaced by the hyperradius $R = (r_1^2 + r_2^2)^{1/2}$, the hyperangle $\alpha = \tan^{-1}(r_1/r_2)$, and Ω which denotes collectively four angles $(\hat{r}_1, \hat{r}_2)$. R represents the overall size of the electron pair while α represents relative radial distances of two electrons from the nucleus. Expressing the two-electron wavefunction by

$$\psi = \frac{\Psi(R, \alpha, \Omega)}{R^{5/2}\sin\alpha\cos\alpha} \tag{2}$$

and substituting it in (1), one gets for the reduced wavefunction Ψ in the hyperspherical coordinates

$$\left(-\frac{1}{2}\frac{\partial^2}{\partial R^2} + \frac{H_{\rm ad}}{R^2} - E\right)\Psi(R, \alpha, \Omega) = 0. \tag{3}$$

Here the adiabatic Hamiltonian is given by

$$H_{\rm ad}(R; \alpha, \Omega) = \Lambda^2(\alpha) - RC(\alpha, \theta_{12}) \tag{4}$$

with

$$\Lambda^2(\alpha) = \left(-\frac{\partial^2}{\partial\alpha^2} + \frac{l_1^2}{\cos^2\alpha} + \frac{l_2^2}{\sin^2\alpha}\right) - \frac{1}{4} \tag{5}$$

$$C(\alpha, \theta_{12}) = \frac{2Z}{\cos\alpha} + \frac{2Z}{\sin\alpha} - \frac{2}{\sqrt{1 - \sin 2\alpha\cos\theta_{12}}}. \tag{6}$$

θ_{12} is the angle between $\hat{r}_1, \hat{r}_2$ and l_1, l_2 are the individual angular momentum operators for the two electrons.

Treating R as a slowly varying adiabatic parameter, $\Psi(R, \alpha, \Omega)$ can be expressed in the close-coupling expansion by a set of $N_{\rm ch}$ channel functions ϕ_μ at each R

$$\Psi(R, \alpha, \Omega) = \sum_{\mu=1}^{N_{\rm ch}} F_\mu(R)\phi_\mu(R; \alpha, \Omega). \tag{7}$$

2.1. The channel function ϕ_μ and the DBS method

In the standard adiabatic approximation, the channel function ϕ_μ is usually chosen to be the eigenfunction of the adiabatic Hamiltonian:

$$H_{ad}(R;\alpha,\Omega)\phi_\mu(R;\alpha,\Omega) = U_\mu(R)\phi_\mu(R;\alpha,\Omega) \tag{8}$$

where $U_\mu(R)$ is the adiabatic potential. In solving (8) for a given R, the adiabatic channel function ϕ_μ is further expanded by basis functions with the angular part $Y_{l_1 l_2}^{LM}(\Omega)$, the coupled spherical harmonic function formed by angular momentum l_1, l_2 of the two electrons, and functions depending on α, which are often taken in analytic forms (Lin 1986). Equation (8) is then solved as an eigenvalue problem to yield both the adiabatic potentials U_μ and the channel functions ϕ_μ. Substituting (7) back to (3), combined with (8), leads to equations for the hyperradial function $F_\mu(R)$

$$\left(-\frac{\partial^2}{\partial R^2} - U_\mu(R) - 2E\right)F_\mu(R) + \sum_\nu W_{\mu\nu}(R)F_\nu(R) = 0 \qquad (\mu = 1,\ldots,N_{ch}) \tag{9}$$

with the diabatic coupling between adiabatic channels μ, ν

$$W_{\mu\nu} = 2\langle\phi_\mu|\frac{d}{dR}|\phi_\nu\rangle\frac{d}{dR} + \langle\phi_\mu|\frac{d^2}{dR^2}|\phi_\nu\rangle. \tag{10}$$

The fact that derivatives of $\phi_\mu(R;\alpha,\Omega)$ with respect to R are involved in $W_{\mu\nu}$ implies that one has to use very small R grids in order to calculate them accurately. This difficulty becomes more severe in avoided-crossing regions of R.

To remedy this problem, in the diabatic-by-sector (DBS) method, R is partitioned into many small sectors $R_0, R_1, \ldots, R_M$. For a given sector, $R_{i-1} < R < R_i$, the wavefunction is expanded in terms of diabatic channel functions ϕ_μ, which are *independent* of R within the sector,

$$\Psi(R,\alpha,\Omega) = \sum_{\mu=1}^{N_{ch}} F_\mu(R)\phi_\mu(R_i^m;\alpha,\Omega) \qquad (R_{i-1} < R < R_i) \tag{11}$$

where we chose R_i^m to be at the midpoint of the ith sector. It is easy to show that the hyperradial function F_μ now satisfies the following close-coupling equations

$$\left(-\frac{\partial^2}{\partial R^2} - 2E\right)F_\mu(R) + \sum_\nu V_{\mu\nu}(R)F_\nu(R) = 0 \qquad (\mu = 1,\ldots,N_{ch}) \tag{12}$$

where the coupling term $V_{\mu\nu}(R)$ between the channels μ and ν is simply given by

$$\begin{aligned} V_{\mu\nu}(R) &= \frac{2}{R^2}\langle\phi_\mu(R_i^m;\alpha,\Omega)|H_{ad}(R;\alpha,\Omega)|\phi_\nu(R_i^m;\alpha,\Omega)\rangle \\ &= \frac{2}{R^2}\left[A_{\mu\nu}(R_i^m) + RB_{\mu\nu}(R_i^m)\right] \qquad (i = 1,\ldots,M) \end{aligned} \tag{13}$$

with

$$A_{\mu\nu}(R_i^m) = \langle\phi_\mu(R_i^m;\alpha,\Omega)|\Lambda^2(\alpha)|\phi_\nu(R_i^m;\alpha,\Omega)\rangle \tag{14}$$

$$B_{\mu\nu}(R_i^m) = -\langle\phi_\mu(R_i^m;\alpha,\Omega)|C(\alpha,\theta_{12})|\phi_\nu(R_i^m;\alpha,\Omega)\rangle. \tag{15}$$

The brackets indicate integrations over the hyperangle α and the angle Ω. Notice that both A and B are independent of R for a given sector, so the calculation of channel couplings $V_{\mu\nu}$ is greatly simplified compared with $W_{\mu\nu}$ in the adiabatic approximation, as one only needs to calculate them once for each sector. Therefore, simply by stipulating that the channel functions are independent of the hyperradius within each sector, the DBS method avoids the calculation of derivatives of ϕ_μ with respect to R in the standard adiabatic approximation. As a result, the calculation of coupling terms $V_{\mu\nu}$ is much simpler and more accurate.

In principle, one can still use the adiabatic basis function at each R_i^m as the basis function in the DBS method, but disregard its R dependence within a given sector. Nevertheless, for the convenience of matching the channel functions to the asymptotic fragmentation channels, in the present work the channel functions in a sector i are defined, for a pair of angular momenta (l_1^μ, l_2^μ), as

$$\phi_\mu(R_i^m; \alpha, \Omega) = \mathcal{A}h_\mu(R_i^m; \alpha)Y^{LM}_{l_1^\mu l_2^\mu}(\Omega) \qquad (R_{i-1}^m < R < R_i^m) \tag{16}$$

with $\mathcal{A}$ as the antisymmetrization operator and $h_\mu(R_i^m; \alpha)$ is chosen to be the eigenfunction of the diagonal part of the adiabatic Hamiltonian

$$\langle Y^{LM}_{l_1^\mu l_2^\mu} | H_{\rm ad}(R_i^m; \alpha, \Omega) | Y^{LM}_{l_1^\mu l_2^\mu} \rangle h_\mu(R_i^m; \alpha) = u_\mu(R_i^m) h_\mu(R_i^m; \alpha). \tag{17}$$

These eigenfunctions h_μ form an orthogonal basis set for the (l_1^μ, l_2^μ) pair and such functions from different (l_1, l_2) pairs are used to construct the global orthonormal basis functions ϕ_μ in equation (16), for each sector. Therefore we see that the basis or channel index μ identifies not only different (l_1, l_2) pairs but also different eigenfunctions $h(\alpha)$ in equation (17). The latter is characterized by the number of nodes in α, which is related to N, the principal quantum number of the inner electron in the limit $R \to \infty$. The numerical aspect of solving equation (17) has been discussed by Tang *et al* (1992a).

Once channel functions ϕ_μ are obtained, channel couplings $V_{\mu\nu}(R)$ are calculated straightforwardly for each sector. Starting from the innermost sector $i = 1$, the close-coupling equations (12) are integrated from R_{i-1} to R_i to obtain the radial functions F_μ, whose values at the end point R_i will serve as the initial boundary condition for the integration in the next sector. The step size between any two adjacent sectors i and $(i+1)$ is chosen to be small enough to ensure the unitarity of the local transformation matrix

$$T_{\mu\nu}(i \to i+1) = \langle \phi_\mu(R_i^m) | \phi_\nu(R_{i+1}^m) \rangle. \tag{18}$$

The integration propagates from inner sectors to outer ones, until the matching boundary $R = R_M$ is reached. From (12), with $N_{\rm ch}$ linearly independent boundary conditions

$$F_\mu^{(\gamma)}(0) = 0, \; F_\mu'^{(\gamma)}(0) = \delta_{\mu\gamma} \qquad (\gamma = 1, \ldots, N_{\rm ch}) \tag{19}$$

where the prime denotes the derivative with respect to R, one can obtain $N_{\rm ch}$ sets of solutions $F_\mu^{(\gamma)}(R)$ for each channel μ. Thereby one can construct $N_{\rm ch}$ general solutions for any sector $i \leqslant M$

$$\Psi^{(\gamma)}(R, \alpha, \Omega) = \sum_{\mu=1}^{N_{\rm ch}} F_\mu^{(\gamma)}(R)\phi_\mu(R_i^m; \alpha, \Omega) \qquad (\gamma = 1, \ldots, N_{\rm ch}). \tag{20}$$

2.2. Matching at $R = R_M$

Beyond $R = R_M$, the two electrons are well separated and can be described more adequately by the known analytical wavefunctions in the independent electron coordinates r_1, r_2. For the cases considered here ($Z > 1$), in the asymptotic region $R > R_M$, the two-electron wavefunction of energy E can be conveniently written as

$$\psi_E^{(\beta)}(r_1, r_2) = \frac{1}{r_< r_>} \sum_{i=1}^{N_{ch}} \Phi_i(r_<) Y_{l_1 l_2}^{LM}(\Omega)[f_i^E(r_>)\delta_{i\beta} - g_i^E(r_>)K_{i\beta}(E)]$$
$$(\beta = 1, \ldots, N_{ch}). \tag{21}$$

where Φ_i is the bound hydrogenic radial function of nuclear charge Z of the inner electron for channel i characterized by a binding energy $E_i = -\frac{Z^2}{2N(i)^2}$ with $N(i)$ as the inner electron's principal quantum number. The functions f_i, g_i are the energy normalized regular and irregular radial Coulomb functions of charge $(Z-1)$ respectively of the outer electron if channel i is open ($E \geqslant E_i$), or exponentially increasing and decreasing functions if channel i is closed ($E < E_i$).

Similar to the R-matrix method, the reaction matrix $\boldsymbol{K}$ is obtained when the numerical solution and its derivative with respect to R in the inner region are matched with the asymptotic solutions at $R = R_M$. That is,

$$\sum_{\gamma=1}^{N_{ch}} C_{\gamma\beta}\Psi^{(\gamma)}(R_M; \alpha, \Omega) = (R^{5/2}\sin\alpha\cos\alpha)\psi_E^{(\beta)}(r_1, r_2)\Big|_{R=R_M} \tag{22}$$

$$\left[\sum_{\gamma=1}^{N_{ch}} C_{\gamma\beta}\Psi^{(\gamma)}(R; \alpha, \Omega)\right]'_R\Big|_{R=R_M} = \left[(R^{5/2}\sin\alpha\cos\alpha)\psi_E^{(\beta)}(r_1, r_2)\right]'_R\Big|_{R=R_M}. \tag{23}$$

$\boldsymbol{C}$ is a constant ($N_{ch} \times N_{ch}$) matrix. To obtain an expression for the $\boldsymbol{K}$ matrix, the asymptotic solutions $\psi_E^{(\beta)}$ on the right-hand sides of (22) and (23) are transformed from the independent electron coordinates into the hyperspherical coordinates. Then both equations are multiplied by the channel function $\phi_\mu(R_M; \alpha, \Omega)$ and integrated over α and Ω on the $R = R_M$ surface. Substituting the expressions of Ψ and ψ in equations (20), (21) into equations (22), (23) and utilizing the orthonormality of the channel functions ϕ_μ, the K-matrix can be expressed in the following ($N_{ch} \times N_{ch}$) matrix equation

$$\boldsymbol{K} = \frac{\boldsymbol{RN} - \boldsymbol{N}'}{\boldsymbol{RJ} - \boldsymbol{J}'} \tag{24}$$

where $\boldsymbol{R}$ is the logarithmic derivative matrix of the hyperradial function $\boldsymbol{F}$ [$F_{\mu\gamma} = F_\mu^{(\gamma)}(R)$] at the matching point:

$$\boldsymbol{R} = \boldsymbol{F}'\boldsymbol{F}^{-1}\,|_{R=R_M}. \tag{25}$$

Expressions of matrices $\boldsymbol{J}$, $\boldsymbol{N}$, $\boldsymbol{J}'$, $\boldsymbol{N}'$ are given in the appendix.

2.3. Initial and final state wavefunctions

To calculate a bound state wavefunction such as the ground state wavefunction $(1s^2)\ ^1S^e$, one first needs to determine its binding energy. This is achieved by searching for the zeros of the determinant $|K^{-1}(E)|$ when all channels are closed. Once the binding energy E_0 is known, the hyperradial function $F_\mu^I(R)$ of the initial bound state wavefunction $\Psi_I(R, \alpha, \Omega) = \sum_\mu F_\mu^I(R)\phi_\mu(R; \alpha, \Omega)$ can be obtained by integrating the Schrödinger equation with $E = E_0$, as described in 2.1, subject to boundary conditions which represent exponentially decaying waves at $R = R_M$. The number of nodes in the function $F_\mu(R)$ is equal to $(n-1)$, with n as the outer electron's principal quantum number of the state in the Rydberg series μ.

When there are open channels, continuum wavefunctions are calculated at each given energy E, subject to the asymptotic boundary condition which represents oscillatory regular and irregular Coulomb functions, as shown in (21). However, the continuum wavefunctions thus calculated with the asymptotic behaviour given by (21) do not correspond to the physical final states of the photoelectron in photoionization experiment. Instead of (21), the final states should be subjected to the boundary conditions of an incoming wave,

$$\psi_E^{(\beta)}(r_1, r_2) = \frac{1}{r_< r_>} \sum_{i=1}^{N_{ch}} \Phi_i(r_<) Y_{l_1 l_2}^{LM}(\Omega)[f_i^E(r_>)\delta_{i\beta} - g_i^E(r_>)S_{i\beta}^\dagger(E)] \qquad (\beta = 1, \ldots, N_{ch}) \tag{26}$$

where S is the scattering matrix. The energy-normalized final state wavefunction, $\Psi_E(R, \alpha, \Omega) = \sum_\mu F_\mu^E(R)\phi_\mu(R; \alpha, \Omega)$, corresponding to the boundary condition (26), can be obtained by a simple matrix transformation from the wavefunction satisfying the boundary condition (21), as given by Jacobs (1971).

2.4. Photoionization cross sections

For photon energy $\omega = E - E_0$, where E_0 is the binding energy of the initial bound state and E the total energy of the final state, the photoionization cross section, in the length (L) or the acceleration (A) form, are given by

$$\sigma^L(\omega) = \left(\frac{4\pi^2}{c}\right)\omega|D_L|^2 \tag{27}$$

$$\sigma^A(\omega) = \left(\frac{4\pi^2}{c}\right)\frac{|D_A|^2}{\omega^3} \tag{28}$$

with corresponding dipole matrix elements

$$D_L(E) = \sum_{\mu\nu}\int_0^\infty R\,dR\,F_\mu^E(R)F_\nu^I(R)I_{\mu\nu}^L(R) \tag{29}$$

$$D_A(E) = Z\sum_{\mu\nu}\int_0^\infty \frac{dR}{R^2}F_\mu^E(R)F_\nu^I(R)I_{\mu\nu}^A(R) \tag{30}$$

where $F_\mu^I(R)$ and $F_\nu^E(R)$ are hyperradial functions of the initial and final state wavefunctions respectively. $I_{\mu\nu}^G(R)$ $(G = \mathrm{L}$ or $\mathrm{A})$ is the angular integral part as given in detail by Park *et al* (1986).

3. Calculations

The calculation of the photoionization cross section consists of two major stages: firstly the initial bound state wavefunction has to be calculated, then the final continuum state wavefunction as well as the dipole matrix element of the transition from the initial to the final state for different photon energies are calculated. Generally the diabatic sectors are allocated densely in the small R region but sparsely in the outer region. Since the initial bound state wavefunction is concentrated more in the interior of the system while the final continuum wavefunction spreads out, in actual calculations the initial and final wavefunctions are computed with rather different number of sectors and the matching distance R_M. Furthermore, since R scales approximately as $1/Z$, wavefunctions for ions are much closer to the nucleus so the matching point can be taken at smaller distances. For the initial state wavefunction Ψ_I of all three elements, bases of individual electron angular momentum l up to 4 and total 19 of them (containing up to $N = 9$ channels) have been included. For the final state wavefunction, bases of l up to 5 were used while different channel number N_{ch} and matching distance R_M were implemented for different elements. For He, 100 sectors and $R_M = 7.0$ were used for the initial state, while 320 sectors, $R_M = 119.5$ and 20 channels were used in calculating final $^1P^o$ state wavefunctions. For Li^+, 95 sectors and $R_M = 3.45$ are used for the initial state while 290 sectors, $R_M = 74.75$ and 25 channels were used for the final state. For C^{4+}, 65 sectors and $R_M = 1.225$ were used for the initial state while 230 sectors, $R_M = 39.75$ and 30 channels were used for the final state. In the bound state calculation, the range of the matching radius is limited by the divergence of the exponentially growing asymptotic irregular Coulomb function g_l, especially for high Z ions. R_M values for initial bound states mentioned above are the largest possible values obtained in the current scheme. No such problem exists for R_M of final states and we have varied the matching radius R_M and the number of channels N_{ch} for final continuum states to ensure their convergence of the result. It is required that the matching radius of the final state be much larger than the distances occupied by the doubly excited states pertaining to the energy range under consideration. Accordingly the matching radius has to be set further away from the nucleus when calculating the spectrum near a high lying doubly excited state (high N channel) or a higher member (high n) of the Rydberg series of a low N channel.

The accuracy of the present calculation is first demonstrated by comparing the binding energy E_0 of the ground state $(1s^2)\ ^1S^e$, obtained from searching the zeros in $\det|K^{-1}|$, with other theoretical or experimental results. For He, the calculated ground state energy $E_0 = -2.903\,815$, which is to be compared with the 'exact' non-relativistic value $-2.903\,72$ (Freund *et al* 1984), the experimental value $-2.903\,8107$ (Kelly 1982). For Li^+, our calculated energy is $-7.279\,718$, to be compared with the experimental value $-7.280\,389$ (Kelly 1982), and theoretical values $-7.279\,914$ (Ho 1981) and $-7.278\,93$ (Bhatia and Temkin 1983). For C^{4+}, the calculated ground state energy is $-32.426\,356$, to be compared with experimental value $-32.417\,253$ (Kelly 1982). The relative larger discrepancy with the experimental value in the C^{4+} might be attributed to the fact that the matching radius for the initial state is not large enough.

Photoionization cross sections using both length (L) and acceleration (A) forms are calculated in the present work. For He, the two forms agree with each other to better than 1% for all energies considered in the present work. For Li^+ and C^{4+}, they differ at most by about 5% and 25% (especially in the higher energy region) respectively, presumably due to the inaccuracy in initial state wavefunctions which are obtained with small matching radii as restricted by the exponentially growing asymptotic function. Since the A-form weights

more of the smaller R region while the L-form does the opposite, it is believed that the results given by the A-form are more accurate than those given by the L-form. This belief is reinforced by the fact that the photoionization cross section obtained in the A-form shows little change whereas the photoionization cross section of the L-form moves towards the A-form cross section when R_M for the initial state is increased. Thus we will only present the results from the A-form. Fine energy mesh points have been used to scan energy regions where autoionizing resonances are expected.

4. Analysis of resonances

As mentioned in the introduction, a doubly excited state can be classified by a set of approximate quantum numbers K, T, A and N, n. The notation ${}_N(K, T)_n^A$ will be used to designate different doubly excited states. Energy positions E_r and widths Γ of the dominant autoionizing doubly excited states such as the ${}_2(0, 1)_n^+$ series are obtained by fitting the calculated total photoionization cross section near a resonance with the Fano formula, which determines the profile of an 'isolated' autoionization resonance embedded in a continuum background (Fano and Cooper 1965),

$$\sigma_{\text{tot}}(E) = \sigma_0[1 + a(E - E_r)]\left[\rho^2\frac{(q+\epsilon)^2}{1+\epsilon^2} + 1 - \rho^2\right] \tag{31}$$

where $\epsilon = 2(E - E_r)/\Gamma$. Note that a linearly energy dependent background due to the direct photoionization is assumed. The autoionization width Γ, which is the sum of all partial widths to different outgoing channels, can be expressed as

$$\Gamma = \sum_j \Gamma_j = 2\pi \sum_j |\langle \psi_{\text{DES}}|H|\psi_E^j\rangle|^2 \tag{32}$$

where $|\psi_{\text{DES}}\rangle$ is the wavefunction of the autoionizing doubly excited state and $|\psi_E^j\rangle$ is the channel j continuum wavefunction of energy E. H is the two-electron Hamiltonian operator. The matrix element $\langle \psi_{\text{DES}}|H|\psi_E^j\rangle$ measures the interaction between the doubly excited state ψ_{DES} and the outgoing continuum ψ_E^j of channel j. In (31), the parameter ρ^2 is defined as

$$\rho^2 = \frac{\left[\sum_j \langle \psi_{\text{DES}}|H|\psi_E^j\rangle\langle\psi_E^j|z_1 + z_2|\psi_I\rangle\right]^2}{\left[\sum_j |\langle \psi_{\text{DES}}|H|\psi_E^j\rangle|^2\right]\left[\sum_j |\langle \psi_E^j|z_1 + z_2|\psi_I\rangle|^2\right]} \tag{33}$$

which represents the relative strength between two portions of the cross section which correspond respectively to transitions to parts of the continuum that do or do not interact with the resonance state $|\psi_{\text{DES}}\rangle$. The Fano shape parameter q, is given by

$$q = \frac{\langle \psi_{\text{DES}}|z_1 + z_2|\psi_I\rangle + P\int_0^\infty [dE'/(E - E')]\sum_j \langle \psi_{\text{DES}}|H|\psi_{E'}^j\rangle\langle\psi_{E'}^j|z_1 + z_2|\psi_I\rangle}{\pi\sum_j \langle \psi_{\text{DES}}|H|\psi_E^j\rangle\langle\psi_E^j|z_1 + z_2|\psi_I\rangle} \tag{34}$$

where P denotes the principal value integration and the summation over j includes all open channels. By using $(z_1 + z_2)$ in (33) and (34) for the electric dipole transition operator, the photon polarization direction has been assumed to be along the z-axis.

While energy positions E_r and widths Γ of the ${}_2(0, 1)_n^+$ states are obtained by the least-squares fitting of equation (31) with six varying parameters E_r, Γ, σ_0, ρ^2, a and q to the spectra in the neighbourhood of those major resonances, energy positions of other weak and narrow states are estimated simply by zooming in the local resonance energy region. Since these resonances are extremely narrow in width (at least two orders of magnitude smaller than the major ones) energy positions thus determined are still quite accurate.

5. Results and discussion

5.1. Photoionization spectra

In the energy range between the threshold I_{P_1} and I_{P_2}, only $1s\epsilon p$ channel is open. There are three $^1P^o$ series associated with the $N = 2$ manifold, i.e. ${}_2(0, 1)_n^+$ $(n = 2, 3, \ldots)$, ${}_2(1, 0)_n^-$ and ${}_2(-1, 0)_n^0$ $(n = 3, 4, \ldots)$.

Before discussing the photoionization cross sections, let us first note that photon energy ranges between I_{P_1} and I_{P_2} are very different for the three elements, with $24.60 \sim 65.41$ eV for He, $75.64 \sim 167.48$ eV for Li^+ and $392.56 \sim 759.92$ eV for C^{4+}. Moreover, autoionizing resonance structures appear only in the energy regime close to the $N = 2$ threshold I_{P_2}. For instance, the first doubly excited state ${}_2(0, 1)_2^+$, shows up at photon energy of about 60 eV in He, about 150 eV in Li^+ and about 665 eV in C^{4+}. Since the main interest here is in doubly excited states, we have calculated the photoionization cross section starting from an energy just slightly below the energy of the first doubly excited state.

In figure 1, the photoionization cross sections of He, Li^+ and C^{4+} are shown. For easier comparison, we plot the photoionization spectra as a function of the scaled energy, $E^* = (E - I_{P_N})/(Z - 1)^2$. In this case, $N = 2$, thereby $E^* = 0$ corresponds to $E = I_{P_2}$. From the figure, we clearly see prominent resonance structures from the autoionizing doubly excited states which are embedded in a smoothly decreasing single ionization background. We have used the simplified notation K_n^A to designate the different resonance states in the figure and in figures hereafter.

In the following we discuss some features of particular significance, as observed from figure 1.

(i) As in He, the dominant series for both Li^+ and C^{4+} ions is the 0_n^+ $(n = 2, 3, \ldots)$ series. The other two series 1_n^- and $(-1)_n^0$ $(n = 3, 4, \ldots)$ have much narrower widths and are much weaker. This implies that the propensity rule that only the states with $K = N - 2$, $A = +$ are predominantly populated in photoabsorption is still valid here.

(ii) The magnitude of the background cross section decreases with increasing Z. For instance, the cross section at $E^* = -0.25$ decreases from ~ 2 Mb in He to ~ 0.18 Mb in C^{4+}. This is a reflection that I_{P_2} for the higher Z element is larger and most of the oscillator strengths have been taken by the singly excited states.

(iii) Relative positions between different autoionization states shift as the nuclear charge Z varies from 2 to 6. This can be seen more clearly if we expand the energy scale and focus on resonances associated with $n = 3$–6, as done in figure 2. For example, in the He spectrum (figure 2(*a*)), the state $(-1)_n^0$, which is also referred to sometimes as the $2pnd$ state, is very close to the state $1_{(n+1)}^-$ and therefore quite difficult to identify. (We mention that this series has been observed in He experimentally only very recently and the present HSCC method has been applied to examine this series in a separate publication.) But in the case of Li^+ (figure 2(*b*)), these two series are well separated, as the $(-1)_n^0$ states drift to the lower energy side towards the 0_n^+ states while the $1_{(n+1)}^-$ states move toward the $0_{(n+1)}^+$ states in the opposite direction. This trend becomes more obvious in C^{4+} (figure 2(*c*)), where the three states of the same n cluster together in a group $(1_n^-, 0_n^+, -1_n^0)$. It should be noted that the successive order $(1_n^-, 0_n^+, -1_n^0)$ of the energy positions is the same for all elements. This energy splitting, from the largest K to the smallest, is a result of the polarization of the inner electron wavefunction under the influence from the outer one, with the quantum number K being the measure of different polarizabilities of the inner core. For higher Z, groups of resonances belonging to different n become well separated because

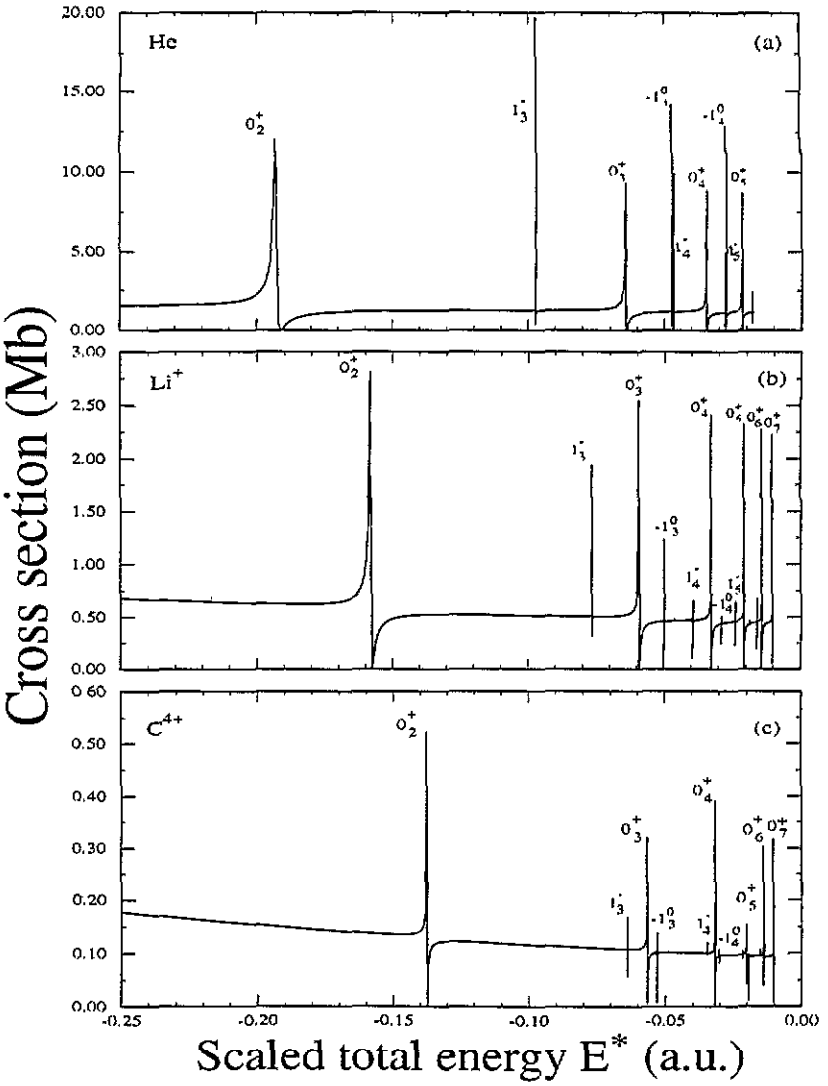

Figure 1. Photoionization cross section below the $N = 2$ threshold plotted against the scaled energy E^*: (*a*) for He; (*b*) Li^+; (*c*) C^{4+}. The autoionizing doubly excited states are denoted by K_n^A.

intershell couplings (from the configuration interaction viewpoint) for these states become negligible.

5.2. Resonance positions and widths

Energy positions and widths of autoionizing states for n up to 6, obtained in the calculation are presented in tables 1–3 for the three elements. Only the widths of the prominent series 0_n^+ are given. In the earlier work (Tang *et al* 1992a), Tang *et al* have determined the energy positions and widths of He doubly excited states using the delay time of the e + He^+ scattering process. The present calculation gives almost the same energy positions while the widths obtained here are also in excellent agreement with the widths tabulated in Tang *et al* (1992a) with less than 2% difference. In tables 1–3 results from some other theoretical

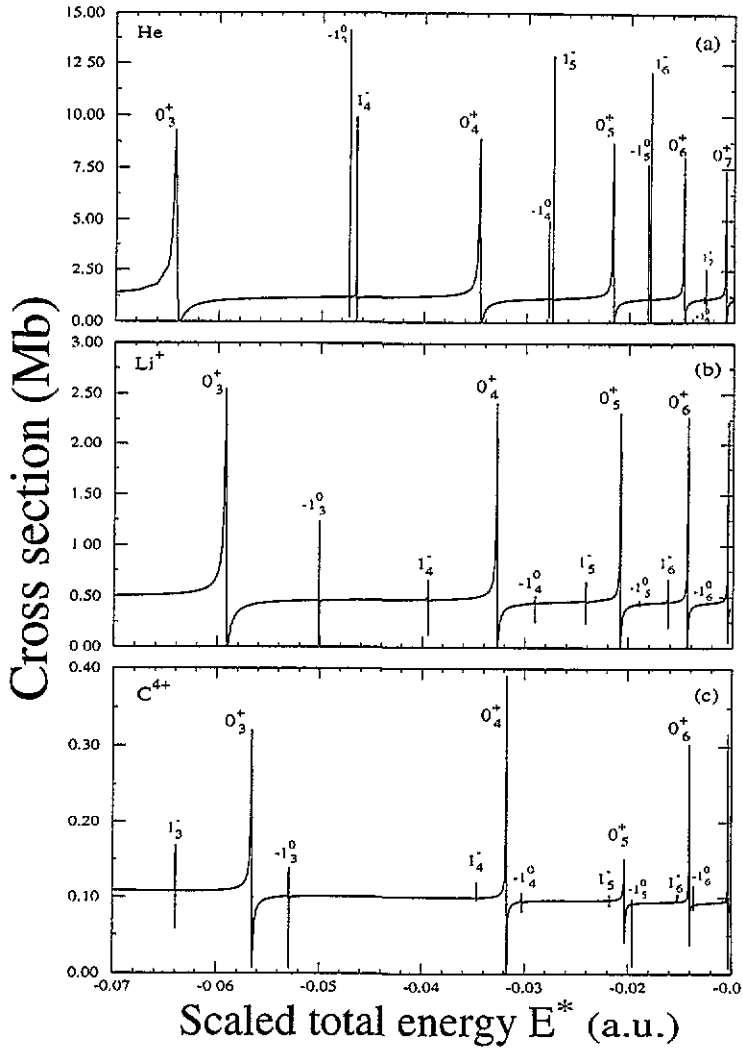

Figure 2. A close-up of the photoionization spectra showing resonance structures near the $n = 3$–6 region: (*a*) for He; (*b*) Li^+; (*c*) C^{4+}.

works are also shown. For He, energy positions and widths calculated in the present work are in excellent agreement with results of the complex coordinate rotation method (CCR) (Ho 1981) and the L^2 basis method (LB) (Sánchez and Martin 1990). The energy positions obtained using the saddle-point technique (Chung and Davis 1980) also agree very well with the present results, while the energy positions predicted by Lipsky *et al* (1977) using the truncated diagonalization method (TD) are considerably higher than other results. For Li^+, energy positions and widths obtained are in excellent agreement with the CCR calculation (Ho 1981) and the LB calculation (Sánchez and Martin 1990). Results obtained using the TD method (Lipsky *et al* 1977) for E_r are again much higher than results of other works. For C^{4+}, the present results are compared with Chen's configuration interaction (CI) calculation (1992), besides the Ho's CCR results (1981). Once again the present results, both the energy positions and the widths of 0_n^+ series, are in excellent agreement with their counterparts of

Table 1. Energy positions and widths $-E_r$ (Γ) in au of He $^1P^o$ resonances below the $N = 2$ threshold.

$_N(K,T)^A_n$	TD[a]	CCR[b]	LB[c]	SP[d]	Present work
$_2(0,1)^+_2$	0.6884	0.6931 (1.37E−3)	0.6929 (1.41E−3)	0.6927	0.6930 (1.39E−3)
$_2(1,0)^-_3$	0.5965	0.5971	0.5972 (4.12E−6)	0.5971	0.5972
$_2(0,1)^+_3$	0.5629	0.5640 (3.00E−4)	0.5640 (3.08E−4)	0.5639	0.5642 (3.01E−4)
$_2(-1,0)^0_3$	0.5468	0.5469	0.5471 (5.77E−8)	0.5470	0.5473
$_2(1,0)^-_4$	0.5462		0.5465 (2.09E−6)	0.5464	0.5467
$_2(0,1)^+_4$	0.5339		0.5344 (1.32E−4)	0.5341	0.5346 (1.28E−4)
$_2(-1,0)^0_4$	0.5275		0.5277 (1.38E−8)	0.5275	0.5279
$_2(1,0)^-_5$	0.5271		0.5274 (1.02E−6)	0.5272	0.5275
$_2(0,1)^+_5$	0.5213		0.5216 (6.87E−5)		0.5217 (6.59E−5)
$_2(-1,0)^0_5$	0.5180		0.5180 (1.05E−9)		0.5183
$_2(1,0)^-_6$	0.5178				0.5180

[a] Lipsky *et al* (1977), the truncated diagonalization method.
[b] Ho (1981), the complex coordinate rotation method.
[c] Sánchez and Martín (1990), the L^2 basis method. The ground state energy $E_0 = -2.903\,72$ au and 1 au(^{4}He) = 27.207 696 eV have been used in the conversion.
[d] Chung and Davis (1980), the saddle-point method.

Table 2. Energy positions and widths $-E_r$ (Γ) in au of Li^+ $^1P^o$ resonances below the $N = 2$ threshold.

$_N(K,T)^A_n$	TD[a]	CCR[b]	LB[c]	Present work
$_2(0,1)^+_2$	1.7473	1.7576 (2.14E−3)	1.7568 (2.29E−3)	1.7574 (2.38E−3)
$_2(1,0)^-_3$	1.4295	1.4307 (6.50E−6)	1.4312 (6.25E−6)	1.4307
$_2(0,1)^+_3$	1.3565	1.3614 (6.60E−4)	1.3617 (7.24E−4)	1.3615 (6.32E−4)
$_2(-1,0)^0_3$	1.3230	1.3252 (4.0E−6)	1.3253 (5.18E−6)	1.3253
$_2(1,0)^-_4$	1.2815		1.2831 (3.29E−6)	1.2829
$_2(0,1)^+_4$	1.2528		1.2559 (3.21E−4)	1.2563 (3.04E−4)
$_2(-1,0)^0_4$	1.2393		1.2411 (2.42E−6)	1.2412
$_2(1,0)^-_5$	1.2203		1.2216 (1.74E−6)	1.2214
$_2(0,1)^+_5$	1.2062		1.2083 (1.67E−4)	1.2082 (1.62E−4)
$_2(-1,0)^0_5$	1.1994		1.2008 (1.29E−6)	1.2006
$_2(1,0)^-_6$	1.1890			1.1899
$_2(0,1)^+_6$	1.1812			1.1824 (9.29E−5)

[a] Lipsky *et al* (1977), the truncated diagonalization method.
[b] Ho (1981), the complex coordinate rotation method.
[c] Sánchez and Martín (1990), the L^2 basis method. The ground state energy $E_0 = -7.280\,389$ au and 1 au ($^7Li^+$) = 27.209 536 eV have been used in the conversion.

Ho, while Chen's CI calculation, which is essentially the same as Lipsky *et al* 's TD method, gives energy positions considerably higher than others. From tables 1–3, one also sees that the widths Γ for the series 0^+_n behave with the expected n^{-3} dependence (Fano and Cooper 1965).

In table 4, the resonance photon energy ω_r, autoionization width Γ, along with parameters q, σ_0, ρ^2 and a, obtained from fitting the Fano profile (31) to the spectra near the most prominent resonance of the 0^+_2 state, are shown for the three elements. Results from some representative theoretical and experimental works, mainly for He and Li^+, are also shown. The present results of resonance positions in terms of the total energy E_r have been converted to the photon energy ω_r in eV in order to be directly compared with other results. In the case of He, not only the energy position ω_r and the autoionization width Γ obtained

Table 3. Energy positions and widths $-E_r$ (Γ) in au of C^{4+} $^1P^o$ states below the $N = 2$ threshold.

$_N(K,T)_n^A$	CI[a]	CCR[b]	Present work
$_2(0,1)_2^+$	7.9205	7.9403 (3.35E−3)	7.9399 (3.36E−3)
$_2(1,0)_3^-$	6.0962	6.0978 (8.15E−6)	6.0981
$_2(0,1)_3^+$	5.8968	5.9132 (1.31E−3)	5.9134 (1.27E−3)
$_2(-1,0)_3^0$	5.8117	5.8230 (3.20E−5)	5.8229
$_2(1,0)_4^-$	5.3631		5.3660
$_2(0,1)_4^+$	5.2807		5.2936 (4.75E−4)
$_2(-1,0)_4^0$	5.2466		5.2562
$_2(1,0)_5^-$	5.0399		5.0433
$_2(0,1)_5^+$	4.9973		5.0072 (3.01E−4)
$_2(-1,0)_5^0$	4.9804		4.9884
$_2(1,0)_6^-$	4.8691		4.8805
$_2(0,1)_6^+$	4.8440		4.8518 (1.98E−4)
$_2(-1,0)_6^0$	4.8346		4.8410

[a] Chen (1992), the configuration interaction method.
[b] Ho (1981), the complex coordinate rotation method.

Table 4. Fano parameters of the $^1P^o$ $_2(0,1)_2^+$ resonance. The numbers in parentheses represent experimental uncertainties.

	ω_r (eV)	Γ (eV)	q	σ_0 (Mb)	a (au^{-1})	ρ^2
He						
Present work	60.154[a]	0.0378[a]	−2.73	1.4011	−0.0098	0.9984
Chang and Tang	60.1825	0.0397	−2.68±0.06	1.40		
Sánchez and Martin (1990)	60.151	0.0383	−2.83	1.374		
Bhatia and Temkin (1983)	60.1450	0.0363	−2.849	1.3845		
Morgan and Ederer (1984)	60.151(10)	0.038(2)	−2.6(3)			
Li^+						
Present work	150.260[b]	0.0648[b]	−1.96	0.5759	−0.4978	1.0029
Sánchez and Martin (1990)	150.295	0.0622	−2.20	0.573		
Bhatia and Temkin (1984)	150.2470	0.0593	−2.199			
Carroll and Kennedy (1977)	150.29(5)	0.075(25)	$-1.5(^{+3}_{-5})$			
C^{4+}						
Present work	666.287[c]	0.0914[c]	−1.74	0.1298	−0.1187	0.9993
Sánchez and Martin (1990)			~ -1.72[d]	$\sim$0.13[d]		

[a] The conversion of 1 au (^{4}He) = 27.207 696 eV is used.
[b] The conversion of 1 au (^{7}Li) = 27.209 536 eV is used.
[c] The conversion of 1 au (^{12}C) = 27.210 418 eV is used.
[d] Taken from figure 3 in (Sánchez and Martin 1990).

in this work are in very good agreement with other works, the Fano shape parameter q, the background cross section σ_0 at the resonance are also very close to the theoretical results given by Sánchez and Martin (1990) and Bhatia and Temkin (1983). A similar situation occurs for the case of Li^+. For C^{4+}, relatively few works exist; the parameter q and σ_0 obtained here appear to agree with those by Sánchez and Martin (1990), judging from values in figure 3 in their paper.

5.3. Z-dependence of σ_0, Γ and q of 0_2^+ resonance

From table 4, some systematic trends of parameters σ_0, Γ and q for the 0_2^+ resonance as

a function of Z can be studied, within the non-relativistic approximation. The background cross section σ_0 at the energy of the resonance decreases from He to C^{4+} with approximate Z^{-2} dependence, in accord with the observed diminishing magnitude of the spectral intensity from figure 1 as mentioned in 5.1. For all three elements, ρ^2 obtained from fitting the resonance profile is almost identical to one, which is expected from (33) as $\rho^2 \equiv 1$ when there is only one open channel. More interestingly, the autoionizing width Γ increases monotonically with Z, from 37.8 meV for He to 64.8 meV for Li^+ and 91.4 meV for C^{4+}. It has been shown that the width increases further for still higher Z to a finite limit of about 133 meV or 0.0049 au for $Z = \infty$ (Ho 1981, Chen and Lin 1989). The Fano parameter q, while negative for all three elements, shows similar behaviour as the autoionization width. It increases markedly with increasing Z, from -2.73 for He, to -1.96 for Li^+ and -1.74 for C^{4+}, rapidly approaching a limit of about -1.7 for $Z = \infty$ (Sánchez and Martin 1990). As seen from figure 1, the change in q value reflects different shapes of the resonance profile from He to C^{4+}.

In the remainder of this subsection, we will try to examine the role of electron–electron correlation in determining the observed Z-dependence of these resonance parameters. One way to incorporate the electron–electron correlation is to express the wavefunction in terms of products of independent electron wavefunctions, i.e. the configuration interaction (CI) expansion. For this particular case, the initial state wavefunction ψ_I, the doubly excited state ψ_{DES} and the (energy normalized) final continuum state ψ_E can be represented as

$$|\psi_I\rangle = a_1|1s1s\rangle + a_2|1s2s\rangle + \dots$$
$$|\psi_{DES}\rangle = |\psi_{0_2^+}\rangle = c_1|2s2p\rangle + c_2|2p2s\rangle + c_3|2s3p\rangle + c_4|2p3s\rangle + c_5|2p3d\rangle + \dots$$
$$|\psi_E\rangle = |1s\epsilon p\rangle.$$

Here $|nln'l'\rangle$ denotes a product of two hydrogenic wavefunctions and $\sum_i |a_i|^2 = \sum_i |c_i|^2 = 1$. For simplicity, we have neglected the configuration interactions in the final continuum state. From the expressions $\sigma_0 = \text{const}\, E|\langle\psi_E|z_1 + z_2|\psi_I\rangle|^2$, $\Gamma = |\langle\psi_E|H|\psi_{DES}\rangle|^2 = |\langle\psi_E|1/r_{12}|\psi_{DES}\rangle|^2$, one immediately sees from scale analysis that the Z dependence for σ_0 is Z^{-2} and that Γ does not explicitly depend on Z, given the fact that the total energy E scales with Z^2, z_i with Z^{-1}, $1/r_{12}$ with Z, discrete wavefunctions scale with $Z^{3/2}$, continuum wavefunctions scale with $Z^{1/2}$ and the integration volume scales with Z^{-6}. Therefore, the Z dependence of the matrix element $\langle\psi_E|1/r_{12}|\psi_{DES}\rangle$ and its width Γ is governed solely by the mixing coefficients c_i, or the electron–electron correlation in the doubly excited state. On the other hand, for large Z, the electron–electron interaction is small compared to the Coulomb attraction of the nucleus that the *intershell* couplings, namely the couplings between states of $n \neq n'$, become negligible. This in turn means $c_i (i \geqslant 3)$ will go to zero when $Z \to \infty$. Obviously magnitudes of c_1, c_2 take their largest values when $Z = \infty$. Since the matrix elements $\langle 1s\epsilon p|1/r_{12}|2l2l'\rangle$ contribute to Γ most significantly compared with other matrix elements $\langle 1s\epsilon p|1/r_{12}|2lnl'\rangle$ $(n \geqslant 3)$, it is clear that Γ should take its largest value in the limit $Z = \infty$.

The Z dependence of the q parameter,

$$q = \frac{\langle\psi_{0_2^+}|z_1 + z_2|\psi_I\rangle + P\int_0^\infty [dE'/(E - E')]\langle\psi_{0_2^+}|H|1s\epsilon' p\rangle\langle 1s\epsilon' p|z_1 + z_2|\psi_I\rangle}{\pi\langle\psi_{0_2^+}|H|1s\epsilon p\rangle\langle 1s\epsilon p|z_1 + z_2|\psi_I\rangle} \tag{35}$$

is related to several matrix elements and therefore is more difficult to explain. However we can at least justify that there is a finite value of q in the $Z = \infty$ limit, using scale

analysis. The contribution from the principal integral term, which has the same explicit Z dependence as the denominator and is usually negligible, should give a finite constant in the limit $Z \to \infty$. For the first term, which corresponds to the dipole transition from the ground state to the doubly excited state, the major configuration $|1s1s\rangle$ in the ground state ψ_I makes no contribution at all to the matrix element $\langle\psi_{0_2^+}|z_1 + z_2|\psi_I\rangle$. Therefore, one may rewrite the matrix element $\langle\psi_{0_2^+}|z_1 + z_2|\psi_I\rangle = (a_2\langle\psi_{0_2^+}|z_1 + z_2|1s2s\rangle + a_3\langle\psi_{0_2^+}|z_1 + z_2|1s3s\rangle + \ldots)$ where the individual matrix elements $\langle\psi_{0_2^+}|z_1 + z_2|nsn's\rangle$ scale with Z^{-1}. Furthermore, the Z dependence of the mixing coefficients a_i $(i = 2, 3, \ldots)$ for the ground state can be shown also to be Z^{-1}, simply from the first-order perturbation theory where $a_i = \langle 1sis|1/r_{12}|1s^2\rangle/(E_i - E_1)$. Given that the matrix element $\langle\psi_{0_2^+}|H|1s\epsilon p\rangle$ in the denominator (which is essentially $\sqrt{\Gamma}$) of (35) scales independently with Z and the other matrix element $\langle 1s\epsilon p|z_1 + z_2|\psi_I\rangle$ in the denominator scales with Z^{-2}, the Z dependence for the first term in q scales off explicitly. In conclusion, both terms in q do not have explicit Z dependence thereby q will go to a finite limit when $Z \to \infty$, a fact which has been demonstrated numerically.

6. Conclusions

We have presented the formulation of the hyperspherical close-coupling (HSCC) method in the context of photoionization of a two-electron atomic system. By employing the diabatic-by-sector technique and the frame transformation at the matching point, the two major problems encountered in the traditional adiabatic approximation in the hyperspherical coordinates are solved. Consequently, the results obtained using the HSCC method, in terms of the energy positions and autoionization widths of doubly excited states, as well as photoionization cross sections, are quite accurate compared with other theoretical and experimental results.

Using the HSCC method, we have conducted a systematic calculation of the photoionization cross section for the two-electron systems of He, Li^+ and C^{4+} in the energy range below the $N = 2$ threshold. We have investigated energy positions and widths of resonances up to $n = 6$ states for all three elements. In particular, resonance parameters of the most prominent state 0_2^+ are studied as functions of Z. We have shown that the diminishing electron–electron interaction, especially the intershell interaction, relative to the increasing electron–nucleus interaction, gives rise to the observed Z dependence of those parameters. However, due to the intrinsic energy degeneracy of hydrogen-like ions, the intrashell electron–electron interaction is still vitally important in describing doubly excited states for very highly charged He-like ions. As a result, the independent electron model is not suitable for any two-electron atomic systems. The results obtained here may serve as a guidance for future experiments on the photoionization of positive He-like ions which become increasingly possible with the recent progress in ion sources.

Acknowledgments

This work was supported in part by the US–Japan Cooperative Research Program sponsored under NSF and JSPS. BZ and CDL were also supported in part by the US Department of Energy, Office of Energy Research, Division of Chemical Sciences.

Appendix

In terms of matrix elements, expressions of J, N, J' and N' are given by

$$J_{\beta\mu} = \int \phi_\mu(R_M;\alpha,\Omega)[\Phi_\beta(r_<)f_\beta(r_>)Y^{LM}_{l_1^\beta l_2^\beta}(\Omega)]\mathrm{d}\alpha\mathrm{d}\Omega \tag{A1a}$$

$$N_{\beta\mu} = \int \phi_\mu(R_M;\alpha,\Omega)[\Phi_\beta(r_<)g_\beta(r_>)Y^{LM}_{l_1^\beta l_2^\beta}(\Omega)]\mathrm{d}\alpha\mathrm{d}\Omega \tag{A1b}$$

$$J'_{\beta\mu} = R_M^{-1/2}\int \phi_\mu(R_M;\alpha,\Omega)\left[R^{1/2}\Phi_\beta(r_<)f_\beta(r_>)Y^{LM}_{l_1^\beta l_2^\beta}(\Omega)\right]'_R\Big|_{R=R_M}\mathrm{d}\alpha\mathrm{d}\Omega \tag{A2a}$$

$$N'_{\beta\mu} = R_M^{-1/2}\int \phi_\mu(R_M;\alpha,\Omega)\left[R^{1/2}\Phi_\beta(r_<)g_\beta(r_>)Y^{LM}_{l_1^\beta l_2^\beta}(\Omega)\right]'_R\Big|_{R=R_M}\mathrm{d}\alpha\mathrm{d}\Omega \tag{A2b}$$

with $\beta,\mu = 1,\ldots,N_{\mathrm{ch}}$. Functions f, g are the regular and irregular Coulomb functions of the outer electron and Φ is the radial hydrogenic function of the inner electron as used in equation (21). Primes on the right-hand side of equation (A2) denote the derivatives with respect to R. $r_>[=\max(r_1,r_2)]$ and $r_<[=\min(r_1,r_2)]$ are expressed at $R = R_{\mathrm{M}}$

$$r_< = R_{\mathrm{M}}\sin\alpha \qquad r_> = R_{\mathrm{M}}\cos\alpha \qquad \text{if } \alpha \leqslant \pi/4 \tag{A3a}$$

or

$$r_< = R_{\mathrm{M}}\cos\alpha \qquad r_> = R_{\mathrm{M}}\sin\alpha \qquad \text{if } \alpha > \pi/4. \tag{A3b}$$

Substituting the basis function

$$\phi_\mu(R_M;\alpha,\Omega) = \sqrt{\tfrac{1}{2}}\left[h_\mu(R_M;\alpha)Y^{LM}_{l_1^\mu l_2^\mu}(\Omega) + (-1)^{l_1^\mu+l_2^\mu-L+S}h_\mu(R_M;\pi/2-\alpha)Y^{LM}_{l_2^\mu l_1^\mu}(\Omega)\right] \tag{A4}$$

into equations (A1) and (A2), after some algebra to eliminate the angular integration over Ω, one obtains

$$J_{\beta\mu} = \int X_{\beta\mu}(R_M;\alpha)\Phi_\beta(r_<)f_\beta(r_>)\mathrm{d}\alpha \tag{A5a}$$

$$N_{\beta\mu} = \int X_{\beta\mu}(R_M;\alpha)\Phi_\beta(r_<)g_\beta(r_>)\mathrm{d}\alpha \tag{A5b}$$

$$J'_{\beta\mu} = \frac{J_{\beta\mu}}{2R_M} + \int X_{\beta\mu}(R_M;\alpha)\left[\Phi'_\beta(r_<)f_\beta(r_>)\left(\frac{\mathrm{d}r_<}{\mathrm{d}R}\right) + \Phi_\beta(r_<)f'_\beta(r_>)\left(\frac{\mathrm{d}r_>}{\mathrm{d}R}\right)\right]_{R=R_{\mathrm{M}}}\mathrm{d}\alpha \tag{A6a}$$

$$N'_{\beta\mu} = \frac{N_{\beta\mu}}{2R_M} + \int X_{\beta\mu}(R_M;\alpha)\left[\Phi'_\beta(r_<)g_\beta(r_>)\left(\frac{\mathrm{d}r_<}{\mathrm{d}R}\right) + \Phi_\beta(r_<)g'_\beta(r_>)\left(\frac{\mathrm{d}r_>}{\mathrm{d}R}\right)\right]_{R=R_{\mathrm{M}}}\mathrm{d}\alpha \tag{A6b}$$

where the function X is given by

$$X_{\beta\mu}(R_M;\alpha) = \sqrt{\tfrac{1}{2}}\left[\delta_{l_1^\beta l_1^\mu}\delta_{l_2^\beta l_2^\mu}h_\mu(R_M;\alpha) + \delta_{l_1^\beta l_2^\mu}\delta_{l_2^\beta l_1^\mu}(-1)^{l_1^\mu+l_2^\mu-L+S}h_\mu(R_M;\pi/2-\alpha)\right] \tag{A7}$$

with

$$\frac{\mathrm{d}r_<}{\mathrm{d}R} = \sin\alpha \qquad \frac{\mathrm{d}r_>}{\mathrm{d}R} = \cos\alpha \qquad \text{if } \alpha \leqslant \pi/4 \tag{A8a}$$

or

$$\frac{\mathrm{d}r_<}{\mathrm{d}R} = \cos\alpha \qquad \frac{\mathrm{d}r_>}{\mathrm{d}R} = \sin\alpha \qquad \text{if } \alpha > \pi/4. \tag{A8b}$$

f', g' and Φ' are derivatives of f, g and Φ respectively.

References

Bachau H, Martin F, Riera A and Yanez M 1991 *At. Data Nucl. Data Tables* **48** 167
Bhatia A K and Temkin A 1983 *Phys. Rev.* A **29** 1895
Carroll P K and Kennedy E T 1977 *Phys. Rev. Lett.* **38** 1068
Chen Z 1992 Private communication
Chen Z and Lin C D 1989 *Phys. Rev.* A **40** 6712
Chung K T 1972 *Phys. Rev.* A **6** 1809
Chung K T and Davis B F 1980 *Phys. Rev.* A **22** 835
Christensen-Dalsgaard B L 1984 *Phys. Rev.* A **29** 2242
Cooper J W, Fano U and Prats F 1963 *Phys. Rev. Lett.* **10** 518
Domke M, Remmers G and Kaindl G 1992 *Phys. Rev. Lett.* **69** 1171
Domke M, Xue C, Puschmann A, Mandel T, Hudson E, Shirley D A, Kaindl G, Green C H, Sadeghpour H R and Pedersen H 1991 *Phys. Rev. Lett.* **66** 1306
Fano U and Cooper J W 1965 *Phys. Rev.* **137** 1364
Freund D E, Huxtable B D and Morgan J D III 1984 *Phys. Rev.* A **29** 980
Herrick D R 1983 *Adv. Chem. Phys.* **52** 1
Ho Y K 1979 *J. Phys. B: At. Mol. Phys.* **12** 387
—— 1981 *Phys. Rev.* A **23** 2137
Ho Y K and Callaway J 1985 *J. Phys. B: At. Mol. Phys.* **18** 3481
Jacobs V 1971 *Phys. Rev.* A **3** 289
Kelly R L 1982 *Atomic and Ionic Spectrum Lines below 2000 Å—H through Ar* ORNL-5922. The Rydberg constants with respective reduced masses of He, Li^+ and C^{4+} are used in the energy conversion from eV to au
Lepetit B, Launay J M and Le Dourneuf M 1986 *Chem. Phys.* **106** 103
Lin C D 1986 *Adv. At. Mol. Phys.* **22** 77
Lindle D W, Ferrett T A, Heimann P A and Shirley D A 1987 *Phys. Rev.* A **36** 2112
Lindle D W *et al* 1985 *Phys. Rev.* A **31** 714
Lipsky L, Anania R and Conneely M J 1977 *At. Data Nucl. Data Tables* **20** 127
Macek J 1968 *J. Phys. B: At. Mol. Phys.* **1** 831
—— 1985 *Phys. Rev.* A **31** 2162
Madden R P and Codling K 1963 *Phys. Rev. Lett.* **10** 516
Moccia R and Spizzo P 1987 *J. Phys. B: At. Mol. Phys.* **20** 1423
—— 1991 *Phys. Rev.* A **43** 2199
Morgan H D and Ederer D L 1984 *Phys. Rev.* A **29** 1901
Park C H, Starace A, Tan J and Lin C D 1986 *Phys. Rev.* A **33** 1000
Sadeghpour H R 1992 *J. Phys. B: At. Mol. Opt. Phys.* **25** L29
Salomonson S, Carter S L and Kelly H P 1989 *Phys. Rev.* A **39** 5111
Sánchez I and Martin F 1990 *J. Phys. B: At. Mol. Opt. Phys.* **23** 4263
Scott P and Burke P G 1984 *J. Phys. B: At. Mol. Phys.* **17** 1321
Tang J Z, Watanabe S and Matsuzawa M 1992a *Phys. Rev.* A **46** 2437
—— 1992b *Phys. Rev.* A **46** 3758
Tang J Z, Watanabe S, Matsuzawa M and Lin C D 1992c *Phys. Rev. Lett.* **69** 1633
Woodruff P R and Samson J A 1982 *Phys. Rev.* A **25** 848
Zhou B and Lin C D 1993 *J. Phys. B: At. Mol. Opt. Phys.* the following paper
Zubek M, King G C, Rutter P M and Read F H 1989 *J. Phys. B: At. Mol. Opt. Phys.* **22** 3411